

Electro-optics and structural peculiarities of liquid crystal–nanoparticle–polymer composites

Oleg V. Yaroshchuk,* Leonid O. Dolgov, and Alexei D. Kiselev
Institute of Physics, NASU, prospect Nauki 46, 03028 Kyiv, Ukraine
 (Received 23 April 2005; published 21 November 2005)

The structural peculiarities and electro-optic performance of liquid crystal (LC)–colloidal nanoparticle (NP)–polymer (P) composites formed by photoinduced phase separation are considered. We classify these materials under two groups according to two limiting cases of polymer morphology. The first group corresponding to small polymer concentration comprises LCs filled with NPs that are stabilized with a polymer network. It is found that, in addition to the light scattering caused by the LC orientational defects, the refractive index mismatch between LC and NP aggregates may significantly affect the electro-optic contrast and its angular characteristics. The second group is represented by polymer dispersed liquid crystals (PDLCs) filled with NPs. It is established that, in the process of photoinduced phase separation of the LC-NP-prepolymer mixture, the nanoparticles are mainly involved with the polymer, serving as building blocks for the polymer matrix. When the aggregation rate of the NPs is high or their size is large, the NPs enhance light scattering in the polymer. For low aggregation rate, NPs modify the effective refractive index and/or the absorption coefficient of the polymer phase without producing any noticeable optical inhomogeneity. Additionally, we found that TiO₂ NPs may cause a photochromic effect, which manifests itself in color changes in the course of the photoinduced phase separation. For PDLCs with optically transparent polymer matrices modified by NPs, it is shown that doping with NPs can be used to control the refractive index ratio of the LC and polymer. In this way one can modify the contrast and substantially reduce the off-axis haze of the PDLC. The observed effects show LC-NP-P composites as materials of considerable promise for LCD and other electro-optic applications.

DOI: [10.1103/PhysRevE.72.051715](https://doi.org/10.1103/PhysRevE.72.051715)

PACS number(s): 42.70.Df, 61.30.Pq, 81.07.Pr, 42.79.Kr

I. INTRODUCTION

Electrically controlled light scattering is one of the most fascinating effects in liquid crystals (LCs) exciting great application interest. The devices based on this effect are distinguished by high brightness, simplicity of construction, and wide viewing angle [1]. The light scattering of LCs becomes apparent in polydomain samples. Its efficiency strongly depends on the system composition and morphology. Among many techniques used to enhance light scattering in polydomain LCs, LC doping is the method that has enjoyed the widest application. In this method either the LC is dispersed in a new phase (LCs in porous matrices [2,3], polymer dispersed LCs (PDLCs) [1,4,5]) or, conversely, the new phase is dispersed into the LC (polymer network LCs (PNLCs) [6], LC emulsions [7], and filled LCs [8–17]).

The classical and most comprehensively studied system from this series is the PDLCs. But presently one can observe special interest in filled LCs, because of their simple preparation and wide spectrum of electro-optic properties. This interest is also caused by recent achievements of modern nanotechnologies suggesting a huge number of nanoscale objects that can be potentially used as filling materials for LCs. One of the most intriguing classes of these materials is based on colloidal monodispersed nanoparticles (MNPs) [18]. Using these particles as LC fillers may produce novel properties as compared to conventional LC-aerosil suspensions [8–12]. While the aerosil powder contains primer particle agglomerates, the colloid may contain separated primer nanoparticles

that are stabilized in the liquid. The aggregation of MNPs in LCs may differ from that of powdered NPs. In Ref. [15], Boxel and co-workers investigated electro-optical properties of suspensions of some *organic* monodispersed spheres in liquid crystals. They found that LC-MNP suspensions demonstrate good electro-optic contrast. In addition, colloidal MNPs form a rather strong network in LC layers, which prevents pouring effects in the cells [16].

Our general goal is to study properties of LC suspensions based on *inorganic* nanoparticles. The choice of the inorganic MNPs is motivated by their specific optical, electrical, and surface properties, which may result in the development of qualitatively new composite materials. It is well known that the refractive index of inorganic oxides can be varied over a wide range. One can expect that the refractive index mismatch between inorganic MNPs and LCs may significantly influence the scattering properties of LC-MNP composites. MNPs of inorganic semiconductors may bring interesting electric properties to LCs (for instance, pronounced photo- and thermal electrical conductivity). Because of the active surface of MNPs, some LC-MNP composites may be characterized by strong interfacial interaction, including reactive interaction of these components. Furthermore, it is relatively simple to disperse inorganic colloidal NPs in a LC. Indeed, in contrast to organic particles, the inorganic ones are usually stable in organic solvents, which can be easily replaced by a liquid crystal with lower volatility. In spite of all these advantages, we found only one publication devoted to LCs filled with inorganic colloidal MNPs [17].

As the first step, we study the electro-optic performance of LC-MNP composites. Several types of MNP with distinctly different refractive indices are used. Taking into account the poor stability of pure LC-MNP suspensions [19],

*Corresponding author. Email address: olegyar@iop.kiev.ua

TABLE I. Characteristics of nanoparticles used for making composites.

Particle sort	Particle size (nm)	Refractive index	Density (g/cm ³)	Crystal phase	Particle shape	Form in which particles are obtained	Producer
Sb ₂ O ₅ MNP	7–11	1.7	3.78		Spherical	Dispersion in methanol (30 wt %)	Nissan Chemicals Industries (USA)
SiO ₂ MNP	10–20	1.46	2.26		Spherical	Dispersion in methanol (30 wt %)	Nissan Chemicals Industries (USA)
TiO ₂ MNP	5–10	2.55	4.1	Anatase	Nearly spherical	Dispersion in ethanol (30 wt %)	ANP (Korea)
TiO ₂ NP	25–51	2.55	4.1	80% anatase/20% rutile	Nearly spherical	Powder	Nanophase

our main concern is composites stabilized by polymer (P) structure. Samples with various polymer concentrations are studied. This allows us to elucidate the influence of MNPs on the electro-optics and structural peculiarities of well-known LC-polymer composites, such as PNLCs and PDLCs. The potential of three-component composites LC-MNP-polymer for applications is discussed.

II. EXPERIMENTAL PART

A. Samples

As MNP filler we used several types of colloidal MNP: (1) Antimony pentoxide (Sb₂O₅) MNPs with the size of 7–11 nm; (2) silica (SiO₂) MNPs with the size of 10–20 nm; and (3) titanium dioxide (TiO₂) MNPs with the size of 5–10 nm. The Sb₂O₅ and SiO₂ MNPs were obtained from Nissan Chemicals Industries Ltd. (USA) as colloidal dispersions in methanol with particle content of 35 and 30 wt %, respectively. TiO₂ particles produced by ANP Ltd. (Korea) were obtained as a colloidal dispersion in ethanol (content of particles was about 30 wt %). In some additional experiments we also used TiO₂ nanoparticles with the size of 25–50 nm in the form of powder obtained from Nanophase Inc. (USA). The choice of all these objects is caused by substantial differences in their refractive indices, Table I.

As liquid crystal, the nematic mixture E7 from Merck was used. As photopolymerizing material we employed uv curable adhesive No65 from Norland Inc. (USA). The E7 and Norland's photopolymer No65 were widely used before to prepare LC-polymer composites [12,20–23].

The LC-MNP-P composites were prepared as follows. At first the LC was thoroughly mixed with the colloidal dispersion of MNPs. The intensive mixing caused evaporation of alcohol and, hence, substitution of alcohol with LC in the suspension. The complete removing of alcohol was achieved by applying a vacuum to the suspension at 10⁻² Torr over 0.5 h. As the next step, the prepolymer composition was added to the E7-MNP suspension. The components were mixed under red light to avoid polymerization not desirable at this stage. Mixtures with different concentrations of MNPs and P were prepared. We operated with the volume concentrations of MNP, φ_{MNP} , and polymer, φ_P for reasons discussed later on. The φ_{MNP} and φ_P concentrations were calculated as $\varphi_{MNP} = (m_{MNP}/\rho_{MNP}) / (m_{MNP}/\rho_{MNP} + m_P/\rho_P + m_{LC}/\rho_{LC})$ and $\varphi_P = (m_P/\rho_P) / (m_{MNP}/\rho_{MNP} + m_P/\rho_P$

+ m_{LC}/ρ_{LC}), where m_{MNP} , m_P , and m_{LC} are the masses, while ρ_{MNP} , ρ_P , and ρ_{LC} are the densities of the corresponding phases. In our experiments, the concentration of MNP was kept relatively low ($\varphi_{MNP} = 1–18$ vol %), while the polymer concentration was varied over a wide range ($\varphi_P = 5–50$ vol %). For composites with high polymer content, we chose a small content of MNPs to prevent strong disturbance of the polymer morphology in the composites.

A small amount of spacer ($d = 25$ μ m) was introduced into the mixtures to fix the thickness of the tested layers. The drop of suspension was placed between two glass substrates covered with indium tin oxide layers from the inner side. The substrates were pressed and glued with an epoxy glue. The samples containing prepolymer were irradiated with the full spectrum of a high pressure mercury lamp (100 mW/cm², 20 min), in order to provide photopolymerization and corresponding structuring of the polymer phase. The time period between suspension mixing and sample exposure was reduced to 10 min to minimize aggregation of the MNPs.

B. Methods

The electro-optic characteristics were measured by the measuring system earlier described in Ref. [12]. In this setup, the LC cell is powered by a sinelike voltage signal 0–200 V generated by computer and, subsequently, amplified. The system allowed us to vary both the intensity and the frequency of the applied voltage. There are several types of curves measured in our experiments.

1. Transmittance vs applied voltage curves

The sample transmittance was defined as the ratio $T = I_{out}/I_{in}$, where I_{in} and I_{out} are the intensities of the probe beam before and after passing through the sample. In the latter case, nonscattered light and the light scattered within an angle of 2° were detected with a photodiode. The T - U curves were measured twice: by stepwise voltage increase and, subsequently, by stepwise voltage decrease. In these measurements, the voltage was varied in the range of 0–200 V, whereas the frequency was fixed at 2 kHz.

The typical T - U curves are demonstrated in Fig. 1. When the applied voltage increases, the transmittance of the samples reaches the saturation level T_s . The driving voltage $U_{0.9}$ is defined as the voltage at which T reaches $0.9T_s$. When the voltage goes back to zero, the system generally comes

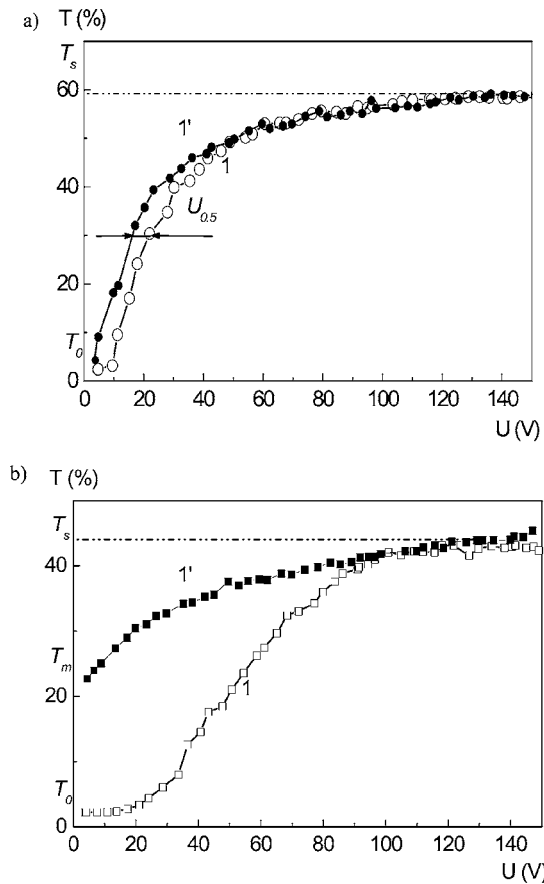


FIG. 1. T - U curves for Sb_2O_5 MNP based composites. The case (a) corresponds to stabilized composite ($\varphi_{\text{Sb}_2\text{O}_5}=2.9$ vol %, $\varphi_P=10$ vol %), and the case (b) to the composite nonstabilized with polymer ($\varphi_{\text{Sb}_2\text{O}_5}=2.9$ vol %). Curves 1 and 1' correspond to voltage ramping on and off, respectively.

into the state with residual transmittance T_m ($T_m \geq T_0$). The ratio $\mathcal{R}=T_s/T_0$ is commonly known as the switching contrast. This parameter is strongly influenced by the initial transmittance, which is the denominator of the fraction.

The curves 1 and 1' from Fig. 1(a) illustrate the case when $T_m=T_0$ and the electro-optic response is thus completely reversible. Figure 1(b) shows the opposite case when the cell possesses electro-optic memory with $T_m \neq T_0$. The pronounced hysteresis can be characterized by $U_{0.5}$ measured as the width of the hysteresis loop at $T=0.5T_s$.

2. Transmittance vs applied voltage frequency curves

The T vs f dependencies ($U=\text{const}$) have been obtained using the oscilloscope program. The transmittance variation under the applied sinusoidal voltage consists of an alternative T_a , and a direct T_d , component. The typical T_a - f , T_d - f , and $T=(T_a+T_d)$ - f curves are represented in Fig. 2. The $T_a(f)$ curve decreases whereas the $T_d(f)$ curve grows monotonically with increasing field frequency. In contrast, the total transmittance is practically constant. Similar results were previously obtained for LC-aerosil and LC-aerosil-polymer composites [10–12]. The T_a component was assigned to the LC domains capable of reorienting in time with the change

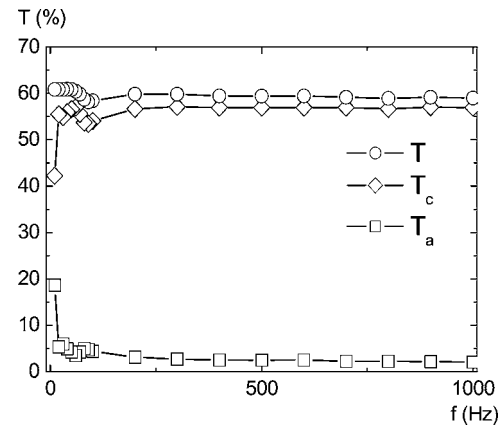


FIG. 2. T , T_a , and T_d vs f curves for E7- Sb_2O_5 -P sample ($\varphi_{\text{Sb}_2\text{O}_5}=2.9$ vol %, $\varphi_P=10$ vol %). $U=17$ V. The lines are guides for the eye.

of electric field. In turn, the T_d component was attributed to large domains, which cannot respond in time with the electric field alternation. The constant value of T can be explained by assuming a fixed amount of LC domains. According to this model the observed decrease of T_a and simultaneous increase of T_d with the field frequency f can be interpreted as diminution of the part of the LC domains reorienting in time with the changes of electric field. The relaxation frequency f_r was estimated as the frequency corresponding to 0.9 decay of T_a . The f_r value was used to estimate the switching on time as $\tau_{on}=1/f_r$.

3. Switching on and switching off kinetic curves

The kinetic curves corresponding to stepwise switching on and switching off the applied voltage have been measured. The decay curve $T(t)$ was used to estimate the decay time τ_{off} as the time of 0.9 decay of T . From the $T(t)$ rise curve the rise time τ_{on} can be roughly estimated to be less than 40 ms. This result is in good agreement with the estimate derived from the relaxation frequency.

4. Transmittance vs incidence angle curves

In these experiments the sample was powered by the saturation voltage and its transmittance was measured as a function of the incidence angle of the laser beam ($\lambda=0.63 \mu\text{m}$). The polarization of the laser beam was in the incidence plane. The reflection losses were estimated by measuring the intensity of the reflected light for various angles of light incidence.

III. RESULTS AND DISCUSSION

The electro-optic characteristics introduced in Sec. II B were measured for a series of samples covering a wide range of component concentrations. The concentration dependencies for three-component composites are more complicated than for two-component ones, since they are functions of two independent parameters, say φ_{MNP} and φ_P . Methodologically, it is convenient to fix the concentrations of two components and consider changes of system properties as the concentra-

tion of the third component varies. In our subsequent considerations of LC-MNP-P composites, the concentrations of the LC and P are fixed and the modification of LC-P composites by MNPs is considered. It is well known that the morphology of LC-P composites depends on the polymer concentration φ_p . At small polymer content (3–10 vol %), the polymer phase typically forms a rigid network (PNLC morphology) [6] while at higher concentrations ($\varphi_p=30\text{--}60$ vol %) it is organized as a porous matrix filled with LC (PDLC morphology) [1,4,5]. The previous studies of LC-P composites based on our components [20,21,24] fully confirm the structural peculiarities described above. So LC-MNP-P composites can be regarded as LC-P systems with PNLC and PDLC morphologies modified by MNPs. As we have verified [25], small amounts of MNP ($\varphi_{MNP} < 10$ vol %) do not change drastically the morphology of LC-P composites so that the suggested classification is reasonable. Section III A elucidates electro-optic characteristics obtained for these two types of LC-MNP-P composites. In Sec. III B, we present both experimental and theoretical results on angular characteristics of LC-MNP-P composites.

A. Electro-optic characteristics: Normal light incidence

1. Electro-optics of polymer stabilized LC-MNP composites

As far as the properties of LC-MNP composites are concerned we concentrate on the most comprehensively studied cases of the E7-Sb₂O₅ and E7-SiO₂ series. The transmittance vs voltage curves for polymer stabilized E7-Sb₂O₅ composites are presented in Fig. 1(a) with curves 1 and 1' (step-up and step-down voltage scans, respectively). For comparison, T - U curves for the nonstabilized E7-Sb₂O₅ suspensions are presented too in Fig. 1(b) (curves 1 and 1'). Similarly to LC-aerosil composites previously investigated in Refs. [8–10], these results indicate effective electro-optic memory of nonstabilized suspensions. By contrast, polymer stabilized samples are virtually free from memory though their T - U curves demonstrate an insignificant hysteresis. In addition, the samples stabilized with polymer show higher electro-optic contrast (by a factor 2–5 as compared with nonstabilized analogs). As shown in Ref. [19], the poorer contrast of the nonstabilized LC-MNP suspension is caused by aggregation and reactive fusion of the MNPs in a liquid crystal, which is not as good a MNP stabilizer as polar organic solvents. The polymer network formed in the LC-MNP suspension prevents separation of a solid phase and thus stabilizes a highly dispersive state of MNPs. In what follows, our attention is focused on the polymer stabilized samples that are characterized by enhanced stability and electro-optic contrast, making them especially attractive for applications.

The dependencies of T_0 , T_s , and \mathcal{R} on the MNP concentration φ_{MNP} are shown in Fig. 3. Figures 3(a) and 3(b) correspond to polymer stabilized E7-Sb₂O₅ and E7-SiO₂ series, respectively. As the MNP concentration increases, T_0 declines for both series of samples. T_s also decreases with increasing φ_{MNP} . The decrease of the $T_s(\varphi_{MNP})$ curve is especially pronounced for the E7-Sb₂O₅ series. This explains the low contrast values obtained for E7-Sb₂O₅ samples. The maximal \mathcal{R} value 14:1 achieved for these composites is 13

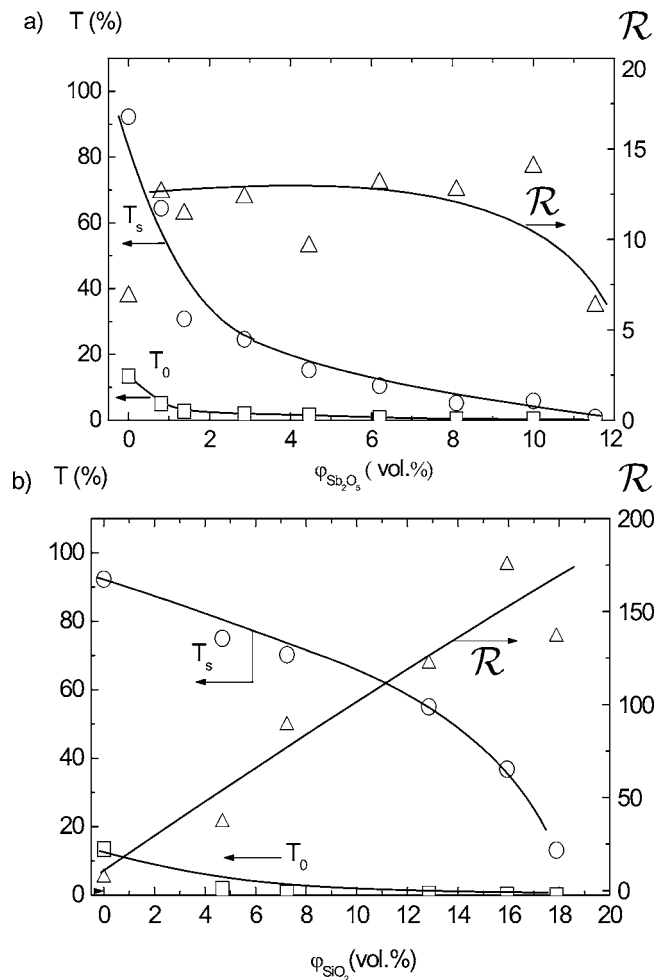


FIG. 3. T_0 , T_s , and \mathcal{R} vs φ_{MNP} curves for polymer stabilized E7-Sb₂O₅ (a) and E7-SiO₂ (b) composites. Polymer concentration is 5 vol %. The lines are just a guide for the eye.

times smaller than for the E7-SiO₂ samples. Qualitatively, the results for E7-TiO₂ series are similar to those for E7-Sb₂O₅ composites except for the steeper decrease of $T_0(\varphi_{MNP})$ and, especially, the $T_s(\varphi_{MNP})$ curve.

The difference in the contrast ratio between E7-Sb₂O₅ and E7-SiO₂ composites can be variously explained. First of all, it may be caused by different aggregation rates of MNPs of various types. This difference, however, should not be considerable in the polymer stabilized samples. In agreement with this, we have not found any substantial difference in the textures of E7-Sb₂O₅ and E7-SiO₂ samples observed by polarizing microscope (see Fig. 4). These textures have very similar grained structure with the size of the largest grains about 10 μm . Assuming that no grain structure is observed for the LC-P samples ($\varphi_p=5$ vol %), one can conclude that these grains correspond to MNP aggregates surrounded by LC. Since the grain sizes are comparable to and higher than the wavelength of the testing light ($\lambda_r=0.63$ μm), one can assume that, together with LC orientational defects, the refractive index jump at the border separating LC and MNP aggregates is an important factor for light scattering in polymer stabilized LC-MNP composites. As we show below, it

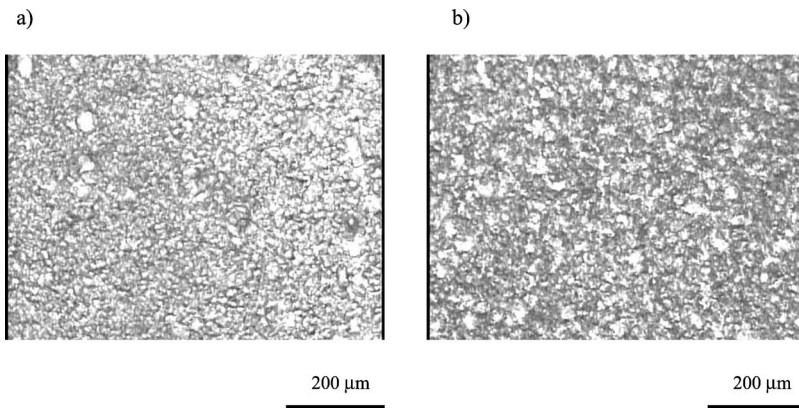


FIG. 4. Microscope photos of polymer stabilized E7-Sb₂O₅ (a) and E7-SiO₂ (b) composites. $\varphi_P=5$ vol %, $\varphi_{MNP}=10$ vol %.

may explain the difference in electro-optic results obtained for the E7-Sb₂O₅ and E7-SiO₂ series.

Let us consider the refractive index diagram of the materials used in our studies (Fig. 5). One can see that the refractive indices of the MNPs are differently removed from the principal refractive indices of the LC. The refractive index of SiO₂ ($n_{SiO_2}=1.46$) lies near the ordinary refractive index of E7 ($n_{LC}^o=1.52$). The refractive index of Sb₂O₅ ($n_{Sb_2O_5}=1.7$) is close to the extraordinary refractive index of E7 ($n_{LC}^e=1.74$). Finally, the refractive index of TiO₂ ($n_{TiO_2}=2.55$) is well above both n_{LC}^o and n_{LC}^e . Thus, from the results for particles of different sorts one can judge the role of the refractive index mismatch in the light scattering by LC-MNP composites.

The light scattering caused by the refractive index mismatch of coexisting LC and MNPs should play a large part for LC-MNP suspensions in transparent states, where the LC orientational defects disappear. First of all, it is worthwhile to compare the transparencies T_s in the saturation state, in which $n_{LC}=n_{LC}^o$ (normal light incidence). In this state, the difference in the refractive index of LC and MNPs is small for SiO₂ particles ($n_{LC}^o-n_{SiO_2}=0.06$) and large for Sb₂O₅ and TiO₂ particles ($n_{Sb_2O_5}-n_{LC}^o=0.18$ and $n_{TiO_2}-n_{LC}^o=2.55-1.52=1.03$, respectively). The high value of the refractive index mismatch in the case of E7-TiO₂ and E7-Sb₂O₅ composites should cause intensive light scattering in the on state. By contrast, the light scattering in E7-SiO₂ composites should be low. The behavior of $T_s(\varphi_{MNP})$ curves shown in Fig. 3 fully confirms this assumption.

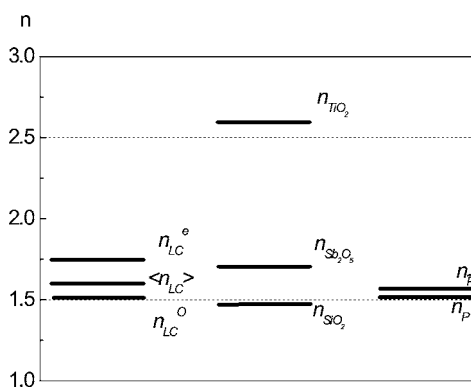


FIG. 5. The refractive index diagram for the components of the studied composites.

The light scattering by the refractive index mismatch should also be evident in the isotropic phase. Indeed, we did not observe destruction of the structural grains (Fig. 4) under the phase transition and, therefore, MNP aggregates persist in the isotropic state. Owing to the absence of LC orientational defects, the refractive index mismatch can be reasonably considered as a major factor responsible for light scattering in the isotropic phase.

The temperature of the nematic-isotropic transition of the LC E7 is about 60 °C. For E7-Sb₂O₅ samples ($\varphi_{MNP}=4$ vol %) stabilized at 70 °C we obtained $T_i=72\%$. It is interesting to compare this value with the value of the saturation transmittance at room temperature, $T_s=28\%$. The inequality $T_i>T_s$ can be easily explained from the point of view of the refractive index mismatch of LC and MNPs. In the isotropic state, $n_{LC}=\langle n_{LC} \rangle = \frac{1}{3}(2n_{LC}^o+n_{LC}^e)=1.59$. The value $n_{Sb_2O_5}-\langle n_{LC} \rangle = 1.72-1.59=0.13$ is much smaller than the value $n_{Sb_2O_5}-n_{LC}^o=1.72-1.5=0.22$. This implies that the optical transmittance of the isotropic phase is higher. For E7-SiO₂ composites ($\varphi_{MNP}=4$ vol %), we obtained $T_i=25\%$ and $T_s=75\%$. The corresponding inequality $T_s>T_i$ is in good agreement with the refractive index model discussed. Indeed, $\langle n_{LC} \rangle - n_{SiO_2} = 1.59-1.46=0.13$ is larger than $n_{LC}^o - n_{SiO_2} = 1.52-1.46=0.06$.

In the field off state, the light scattering caused by orientational defects masks the contribution from the refractive index mismatch. Assuming that the LC is randomly oriented, i.e., $n_{LC}=\langle n_{LC} \rangle$, one can deduce that the contribution of the refractive index mismatch is similar to the contribution in the isotropic state. So it enhances light scattering at 1–10 % depending on the particle type and the particle concentration.

With increasing MNP concentration the controlling voltage $U_{0.9}$ and the hysteresis value $U_{0.5}$ gradually increase, while the response times τ_{on} and τ_{off} decrease (see Fig. 6). These results are in good agreement with earlier studies of LC-aerosil mixtures [11,12] and can be explained by diminishing LC domains separated by the MNP network. For more details on the kinetic characteristics of LC-MNP-P composites we refer readers to our previous publication [26].

2. Electro-optics and structure of PDLC filled with MNPs

We begin with the properties of nondoped PDLCs based on the chosen components. We present only \mathcal{R} , $U_{0.9}$, and τ_{off} vs φ_P curves that are essential for further explanations

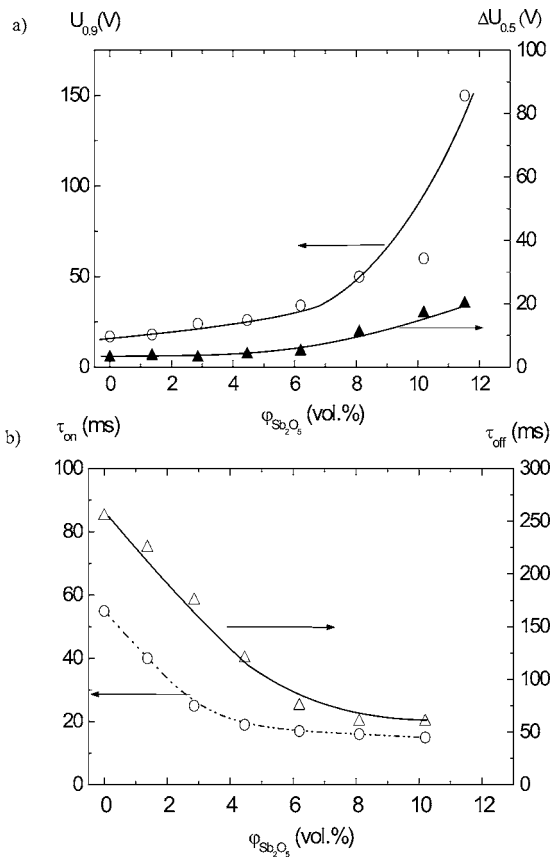


FIG. 6. $U_{0.9}, \Delta U_{0.5}$ (a) and τ_{on}, τ_{off} (b) as functions of MNP concentration for polymer stabilized E7-Sb₂O₅ composites ($\varphi_P = 5$ vol %). The lines are guides for the eye.

(curve 1 in Figs. 7, 8, and 9, respectively). The increasing character of the $\mathcal{R}(\varphi_P)$ curve before reaching its maximum at about 40 vol % means that the PDLC morphology is effectively formed at $\varphi_P \approx 40$ vol % of prepolymer. This conclusion is in agreement with the data of other authors [20,23]. A subsequent decrease of the $\mathcal{R}(\varphi_P)$ curve is mainly caused by strong diminution of the number of LC inclusions playing the role of scattering centers [27].

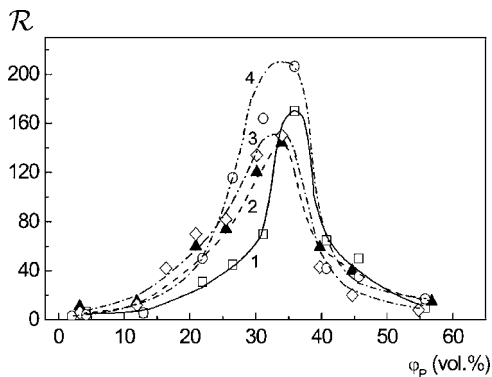


FIG. 7. \mathcal{R} vs polymer concentration curves for E7-MNP-polymer composites. 1, $\varphi_{MNP} = 0$ vol %; 2, $\varphi_{Sb_2O_5} = 1$ vol %; 3, $\varphi_{SiO_2} = 1$ vol %; 4, $\varphi_{TiO_2} = 0.5$ vol % (powder). The concentrations of MNP are optimized for maximal contrast and sample uniformity. The lines are just for guidance.

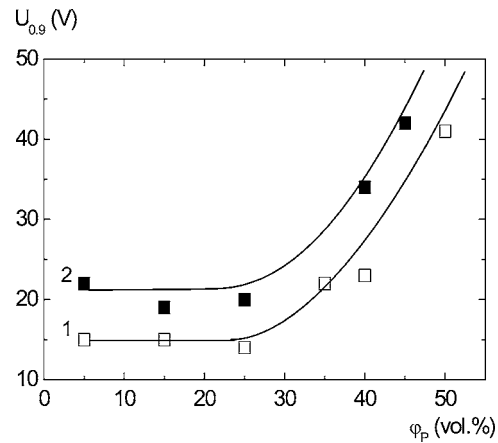


FIG. 8. $U_{0.9}$ vs φ_P curves for E7-P composites, nonfilled (1) and filled with Sb₂O₅ MNP, $\varphi_{Sb_2O_5} = 5$ vol % (2). The lines are guides for the eye.

Visually, LC-P composites filled with Sb₂O₅ and SiO₂ MNPs, similarly to pure LC-P composites, look milky white. By contrast, the samples containing colloidal TiO₂ particles are yellow colored. Additionally, if the phase separation in LC-TiO₂-prepolymer mixtures is stimulated by high intensity irradiation ($I \geq 200$ mW/cm²) of a mercury lamp, the color of the formed composites becomes dark blue. These coloring effects are discussed below.

Figure 7 shows $\mathcal{R}(\varphi_{MNP})$ curves for both pure E7-P composites and composites filled with particles of various sorts. It can be seen that doping with MNPs shifts the maximum of the $\mathcal{R}(\varphi_{MNP})$ curve to the region of lower polymer concentrations. The maximal value of switching contrast changes, however, nonessentially, except for composites filled with powdered TiO₂ particles. Figures 8 and 9 show typical $U_{0.9}(\varphi_P)$ and $\tau_{off}(\varphi_P)$ curves for E7-P composites nonfilled and filled with MNPs, respectively. As one can see, similarly to the $\mathcal{R}(\varphi_{MNP})$ curve, insertion of MNPs results in the shift of $U_{0.9}(\varphi_P)$ and $\tau_{off}(\varphi_P)$ curves to the lower polymer concentration region.

The results presented in Figs. 7–9 may be explained by assuming that, during phase separation in LC-MNP-P com-

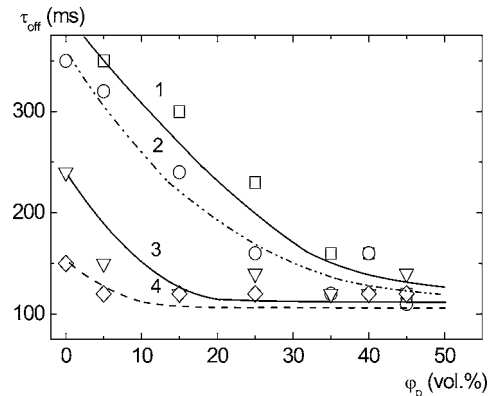


FIG. 9. τ_{off} vs φ_P curves for E7-P composites, nonfilled and filled with Sb₂O₅ MNP. 1, $\varphi_{Sb_2O_5} = 0$ vol %; 2, $\varphi_{Sb_2O_5} = 2.5$ vol %; 3, $\varphi_{Sb_2O_5} = 4$ vol %; 4, $\varphi_{Sb_2O_5} = 5$ vol %. The lines are guides for the eye.

posites, MNPs are mainly involved with the polymer. Moreover, the MNPs can serve as nuclei for polymerization, which grow and merge, forming the polymer phase. In other words, MNPs serve as building blocks for the polymer matrix and so they can be considered as some equivalent amount of polymer. This assumption can also explain the weak change of the maximal contrast obtained by insertion of MNPs in PDLC composites. Indeed, as compared with pure PDLCs, MNPs confined within LC inclusions would generate additional scattering centers leading to substantial increase of the electro-optic contrast.

To confirm the involvement of solid particles with the polymer phase, several experiments were carried out. First, PDLC samples doped with MNPs were kept in hexane to dissolve and remove the LC. The samples were carefully weighed before and after extraction of the LC phase to verify whether MNPs are also removed. We found that the sample lost less weight than the weight of the LC contained in the composite. By observation in the polarizing microscope we also investigated the content of the extracted phase. In these experiments, traces of MNPs were also not found. Finally, the structure of the solid remainder of the MNP doped PDLC was investigated by the scanning electron microscopy (SEM) method. The SEM images did not show evidences of MNPs in the cavities remaining after extraction of the LC [25]. These results confirm the assumption about the preferred involvement of the MNPs with the polymer.

Thus, roughly speaking, doping with MNPs transforms the LC-P system into the LC- \tilde{P} system, where \tilde{P} is the particle modified polymer. The properties of the polymer \tilde{P} may essentially differ from the properties of pure polymer depending on the material, size, and aggregation rate of the particles. First of all, embedded MNPs may modify the optical uniformity of the polymer \tilde{P} . The polymer \tilde{P} becomes opaque, if the size of the particles or the particle aggregates is comparable with the wavelength of light. On the other hand, if the diameter of the nanoparticles (aggregates) is below 100 nm, \tilde{P} can be transparent even at very high loading ($\varphi_{MNP} \approx 20$ vol %) [28,29]. Keeping the transparent state of the polymer, MNPs may substantially modify its refractive index. In good approximation, the refractive index of the modified polymer \tilde{P} is a linear function of MNP concentration:

$$n_{\tilde{P}} = n_P \varphi_P + n_{MNP} \varphi_{MNP}, \quad (1)$$

where φ_P and φ_{MNP} are the volume fractions of polymer and MNP [28]. This method is frequently used to augment the refractive index of the polymer, which typically does not exceed 1.7. Adding MNPs with high n_{MNP} allows us to increase this value by a factor of 2 and more [28,29]. For PDLC composites, modification of n_P may result in significant changes of scattering characteristics due to the light scattering caused by the refractive index mismatch of the coexisting phases.

To model the polymer phase obtained in the process of phase separation of our LC-MNP-P mixtures, P-MNP samples were prepared. In these experiments MNP colloid

and prepolymer were mixed and vacuumed to remove the alcohol in which MNPs are stabilized. The mixture was placed between two glass slides. The thickness of the composite layer was maintained with spacer balls of 25 μm in diameter. These probes were irradiated with uv light at the conditions used to prepare LC-MNP-P composites. We established that the light scattering in all composites based on colloidal MNP particles is negligibly small up to 5–7 vol % of particle loading.

In contrast to the colloidal particles, 5 vol % loading of powdered TiO_2 particles results in considerable light scattering of the polymer layers. This is the result of particle aggregation, since primer particles are only 25–50 nm in diameter and they cannot scatter light intensely. The intense light scattering by the polymer skeleton may explain the enhancement of the contrast in LC-powdered TiO_2 -P composites (see Fig. 7).

Like LC- TiO_2 -P composites, TiO_2 -P composites are yellow colored. This may be caused by chemical reaction of trimethylolpropane trisilol from the prepolymer No65 [30] with TiO_2 filler. The product of this reaction is titanium mercaptide, which has a yellow appearance.

The P- TiO_2 probes cured with intense light ($I \approx 200 \text{ mW/cm}^2$) showed a reversible color change from yellow to dark blue. According to Refs. [31,32], this photochromic effect is caused by the titanium atoms transferring from the IV to III valency state. In our system, strong photochromism may be caused by the transition of titanium mercaptide from the IV [$\text{TiO}(\text{SR})_2$] to III (TiOSR) valency state under the action of uv light. Due to oxidation, titanium III slowly returns back to the titanium IV state, and so the photochromic transition is reversible. The coloring effects observed in our samples might be used to improve the electro-optic contrast of PDLC composites. In addition, PDLCs with a photochromic polymer phase may be attractive objects for information processing systems, nonlinear optics, holography, etc. [33,34].

The modification of the refractive index mismatch of a polymer by MNPs is evident in the change of T_s and T_i values. For instance, for a pure PDLC ($\varphi_P=40$ vol %), $T_s=95\%$ and $T_i=70\%$, while for a PDLC doped with Sb_2O_5 MNPs ($\varphi_P=37$ vol %, $\varphi_{\text{Sb}_2\text{O}_5}=3$ vol %), $T_s=35\%$ and $T_i=51\%$. Thus, $T_s < T_i$ for an Sb_2O_5 doped PDLC, in contrast to the ratio $T_s > T_i$ for a pure PDLC. Qualitatively, these inequalities can be explained by using the refractive index diagram. For the sake of simplification, the diagram in Fig. 5 neglects the solubility of LC and polymer. For a pure PDLC, $n_P \cong n_{LC}^o$ so that T_s value approaches 100%, while $T_i < T_s$. The relation $T_s < T_i$ obtained for an Sb_2O_5 doped PDLC may imply that $n_{\tilde{P}}$ is close to $\langle n_{LC} \rangle$ and so the T_i value is high. The ratios of T_s and T_i obtained for composites based on other types of MNP may also be explained from the viewpoint of the refractive index mismatch of the LC and the modified polymer.

B. Angular characteristics of light transmittance

The angular characteristics of \mathcal{R} of LC devices working in light scattering mode suffer from the problem known as

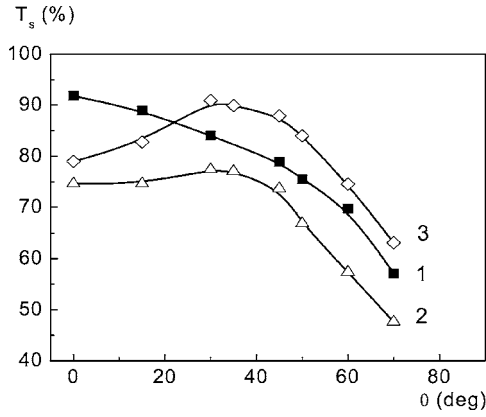


FIG. 10. The sample transmittance (T_s) vs. incidence angle curves for polymer stabilized E7-MNP samples. 1-E7-SiO₂ (φ_{SiO_2} = 0.5 vol. %), 2-E7-TiO₂ (φ_{TiO_2} = 0.5 vol. %), 3-E7-Sb₂O₅ ($\varphi_{\text{Sb}_2\text{O}_5}$ = 0.5 vol. %). For all samples φ_P = 5 vol. %. The lines are just for guidance.

off-axis haze. It lies in the sample hazing on oblique observation in the field on state. For a PDLC, the off-axis haze is caused by the refractive index mismatch of the LC drops and the polymer matrix, if they are matched for normal light incidence ($n_P \approx n_{LC}^o$). The off-axis haze of PDLC can be reduced by selecting the LC and P so as to meet the condition $n_{LC}^o < n_P \ll n_{LC}^e$. In this case refractive index match is achieved at the nonvanishing incidence angle θ (the angle between the normal to the sample and the propagation direction of the testing beam) which results in flattening of the $T_s(\theta)$ curve [4,35]. So far the viewing angle characteristics of filled LCs have not been studied in any detail. In this section, we consider the off-axis haze problem separately because of its importance for applications.

1. Experimental results

We examine the transmittance T_s as a function of the incidence angle θ for light polarized in the incidence plane. For such polarization of light, the refractive index of the LC changes as the cell rotates. Figure 10 presents the $T_s(\theta)$ curves ($U = 120$ V), measured for the polymer stabilized LC-MNP composites. The $T_s(\theta)$ curve for the E7-SiO₂ sample shows a monotonic decrease characteristic of off-axis haze. By contrast, the curves for E7-Sb₂O₅ and E7-TiO₂ composites can be nonmonotonic and rather flat in the range of $\theta < 50^\circ$.

These results can be explained by assuming that the refractive index mismatch between LC and MNP aggregates is responsible for the LC haze. From the Lambert-Beer law, the light scattering is a decaying exponential function of the refractive index mismatch and the optical path length. When the incidence angle increases, the optical path length extends, leading to enhanced light scattering. At the same time, the refractive index difference may go up and down depending on the particle type. In E7-SiO₂ suspensions this value grows with θ , leading to monotonic decrease of the light transmittance. For Sb₂O₅ filler, $n_{\text{Sb}_2\text{O}_5} \approx n_{LC}^e$ and the refractive index difference decreases with decreasing incidence

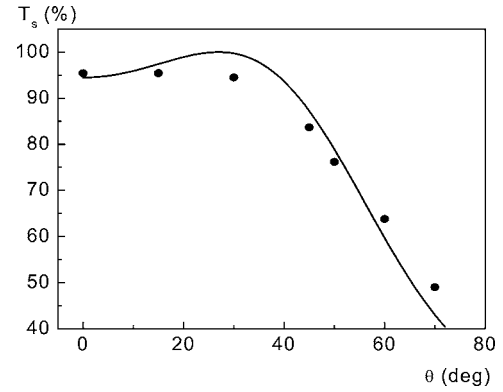


FIG. 11. Transmittance as a function of incidence angle θ for the pure PDLC sample with $\varphi_{LC} = 63$ vol % and $\varphi_{MNP} = 0$. Points correspond to experimental data, solid line represents the theoretical curve computed from Eqs. (7)–(10) at $\varphi_d = 0.44$, $\theta_m = 27^\circ$, and $R_d = 0.35$ μm . The bipolar order parameter S_d and the effective refractive index n_m are estimated at 0.7 and 1.5569, respectively.

angle, approaching zero at grazing angles. The nonmonotonic behavior of the $T_s(\theta)$ curve is due to interplay between two competing factors: lengthening of the optical path and reduction of the refractive index mismatch between LC and MNP which tend to decrease and to increase the transmittance T_s , respectively. In this manner the results for E7-TiO₂ suspensions can also be explained. The observed quantitative difference between E7-TiO₂ and E7-Sb₂O₅ samples (Fig. 10) is caused by the difference in the refractive index mismatch between LC and MNP. This difference can be minimized by fitting concentrations of MNPs.

The transmittance T vs incidence angle θ curves for the LC-P and LC-MNP-P composites of PDLC morphology are presented in Figs. 11 and 12, respectively. It can be seen that the curves for pure PDLC and PDLC filled with SiO₂ are quite steep. By contrast, $T_s(\theta)$ curves of PDLC filled with Sb₂O₅ particles are nonmonotonic and flat enough over the range of 0° – 50° (curves 2 and 3 in Fig. 12).

The $T_s(\theta)$ characteristics of MNP doped PDLCs can be explained by assuming modification of the refractive index of the polymer by MNPs. According to the refractive index diagram (Fig. 5), for a pure PDLC $n_P \approx n_{LC}^o$ so that off-axis haze occurs. Adding SiO₂ particles has almost no effect on the $T_s(\theta)$ characteristic because $n_{\text{SiO}_2} \approx n_{LC}^o \approx n_P$. Doping with Sb₂O₅ particles leads to an increase in the refractive index of the polymer phase \tilde{P} with $n_{LC}^o < n_{\tilde{P}} < n_{LC}^e$. This reduces the off-axis haze, i.e., flattens the $T_s(\theta)$ curve. The reduction of T_s with increasing particle concentration is caused by the additional light scattering due to aggregation of MNPs. The results for the TiO₂ doped PDLC can be explained in the same manner as for the Sb₂O₅ doped samples.

Significant improvement of the $T_s(\theta)$ curve by doping the PDLC with MNPs may be considered as a useful method to reduce the off-axis haze. Using this method, in principle, any polymer can be modified so as to match the LC optically and to get a suitable pair for the PDLC.

2. Theoretical model

Now we discuss the angular dependence of the saturated optical transmittance T_s through samples of PDLC morphol-

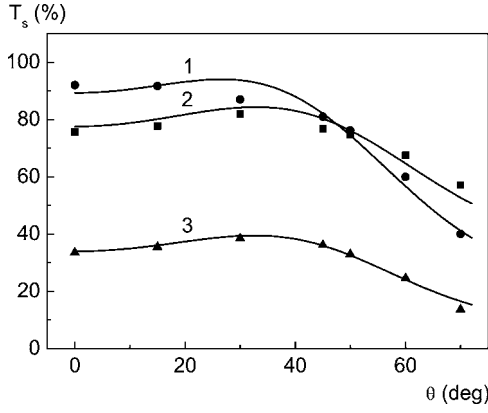


FIG. 12. Transmittance T_s as a function of incidence angle θ for LC-P-MNP samples of PDLC morphology ($\varphi_{LC}=63$ vol %). Points represent experimental data obtained for the samples (1) PDLC doped with SiO_2 MNPs, $\varphi_{MNP}=1.3$ vol %; (2) PDLC doped with Sb_2O_5 MNPs, $\varphi_{MNP}=1.3$ vol %; (3) PDLC doped with Sb_2O_5 MNPs, $\varphi_{MNP}=3.3$ vol %. Solid lines 1–3 represent the theoretical curves computed from Eqs. (7)–(10) at the following values of the fitting parameters: (1) $\theta_m=27^\circ$, $n_m=1.5545$, $\varphi_{MNP}=0.013$, $R_{MNP}=0.2$ μm ; $R_d=0.3$ μm ; (2) $\theta_m=34^\circ$, $n_m=1.5578$, $\varphi_{MNP}=0.013$, $R_{MNP}=0.2$ μm ; $R_d=0.2$ μm ; (3) $\theta_m=36^\circ$, $n_m=1.561$, $\varphi_{MNP}=0.033$, $R_{MNP}=0.4$ μm ; $R_d=0.4$ μm .

ogy using the results and reasons from the previous section and the modified version of the general theoretical approach described in our recent paper [36]. Below, following this approach, we formulate a simple quantitative model and compare the theoretical results with the experimental data obtained for a pure PDLC film and PDLC samples doped with nanoparticles (see Figs. 11 and 12).

As in [36], we assume that the sample without particles can be modeled as an ensemble of spherically shaped nematic droplets and the LC director field \hat{n} inside each droplet forms a bipolar orientational structure. This structure is cylindrically symmetric with the symmetry axis known as the bipolar axis \hat{d} .

As in Refs. [36–39], we shall characterize the optical anisotropy of the droplets using the dielectric tensor averaged over the director distribution inside a droplet. This tensor is uniaxial with the optical axis directed along \hat{d} . Its principal values ε_d^\perp and ε_d^\parallel determine the refractive indices of ordinary and extraordinary waves inside the LC droplets, $n_d^o=\sqrt{\varepsilon_d^\perp}$ and $n_d^e=\sqrt{\varepsilon_d^\parallel}$, which generally differ from the indices of the LC, $n_{LC}^o=\sqrt{\varepsilon_{LC}^\perp}$ and $n_{LC}^e=\sqrt{\varepsilon_{LC}^\parallel}$. This difference is introduced by the averaging and can be conveniently described in terms of the bipolar order parameter Q_d as follows;

$$\varepsilon_d^\perp = \varepsilon_{LC}^\perp + \varepsilon_{LC}^a(1 - Q_d)/3, \quad (2)$$

$$\varepsilon_d^\parallel = \varepsilon_d^\perp + \varepsilon_{LC}^a Q_d, \quad (3)$$

$$Q_d = V_d^{-1} \int_{V_d} [3(\hat{d} \cdot \hat{n})^2 - 1]/2 dV, \quad (4)$$

where $\varepsilon_{LC}^a = \varepsilon_{LC}^\parallel - \varepsilon_{LC}^\perp$ and $V_d = 4\pi R_d^3/3$ is the volume of the droplet.

From Eq. (4) the order parameter Q_d characterizes the degree of droplet anisotropy which depends on distortions of the director field \hat{n} with respect to the configuration uniformly aligned along the bipolar axis \hat{d} . In general, the value of Q_d varies depending on a number of factors such as droplet size and shape, anchoring conditions, applied voltage, and so on. In [40], such variations were found to be negligible and the bipolar order parameter was estimated to be about 0.82. By contrast, the results of [38,41] suggest that the bipolar order parameter of a PDLC film varies considerably depending on the applied electric voltage. Below we find that analysis of the angular dependence of the sample transmittance in the on state provides a method to estimate the bipolar order parameter Q_d .

In our treatment of the light scattering problem we shall also account for the dependent scattering effects by replacing the polymer matrix surrounding the scatterers with an effective medium. For the two-component PDLC system, the refractive index of the medium can be estimated using the simplest mixing rule

$$n_{PDLC} = n_p + \varphi_d(n_d - n_p), \quad (5)$$

where $n_d = (2n_d^o + n_d^e)/3$ is the average refractive index of the LC droplets and φ_d is the volume fraction of the LC droplets in the composite. It should be stressed that the total volume content of the LC in the mixture φ_{LC} differs from the volume fraction of the separated LC droplets φ_d . This difference is caused by solubility of the LC and polymer. The solubility in PDLC composites based on our components was considered in Ref. [23]. Applying the results obtained in [23] to our case of a pure PDLC ($\varphi_{LC}=63$ vol %) we found that the volume fraction φ_d is in the region 41 ± 3 vol %. This is the concentration region for φ_d that was used in our computations.

The relation (5) can be extended to the case of a PDLC doped with MNPs by adding a term proportional to the volume fraction of the particles. So the refractive index of the effective medium takes the following form:

$$n_m = n_{PDLC} + \varphi_{MNP}(n_{MNP} - n_{PDLC}). \quad (6)$$

For the systems under consideration, we found that the relations (5) and (6) give results that agree remarkably well with those derived from other more complicated mixing rules such as versions of the traditional Maxwell-Garnett closure or the modified Bruggeman formula considered in Refs. [36,39,42,43].

The optical transmittance through a film of thickness d is related to the scattering mean free path l_{sca} , which is variously known as the phase coherence length or the extinction length. This length is the characteristic distance between two scattering events after which the phase coherence of radiation gets lost leading to the exponential decay of the incident intensity known as the Lambert-Beer law [44,45]. Thus, the expression for the optical transmittance is given by

$$T_s = \exp[-d(\theta)/l_{sca}(\theta)], \quad (7)$$

where $d(\theta) = n_m d / \sqrt{n_m^2 - \sin^2 \theta} = d / \cos \theta_r$ is the total path length for a plane wave impinging on the film surface at an incidence angle θ . From Snell's law, the wave is refracted at

an angle θ_r inside the sample and $n_m \sin \theta_r = \sin \theta$.

The notation for the transmittance used in Eq. (7) indicates that the applied voltage is high and the system is in the saturated state. In this regime, the bipolar droplets are oriented along the normals to the film substrates, and incoherent scattering is suppressed [36,40].

By using the low concentration approximation we can generalize the result for the scattering mean free path obtained in [36] for a pure PDLC to the case of PDLC-MNP films. For incident light linearly polarized in the incidence plane, we have

$$\Gamma_{sca}^{-1}(\theta) = \rho_d \sigma_d(\theta) + \rho_{MNP} \sigma_{MNP}, \quad (8)$$

$$\sigma_{d,MNP} = 2\pi R_{d,MNP}^2 F[2kR_{d,MNP}(m_{d,MNP} - 1)], \quad (9)$$

$$\frac{1}{m_d^2(\theta)} = \frac{1}{(m^\circ)^2} + \sin^2 \theta \left(\frac{1}{(n_d^e)^2} - \frac{1}{(n_d^o)^2} \right), \quad (10)$$

where $\rho_d = \varphi_d/V_d$ and $\rho_{MNP} = \varphi_{MNP}/V_{MNP}$ are the number densities of the droplets and the particles, respectively, $m^\circ = n_d^o/n_m$, $m_{d,MNP} = n_{d,MNP}/n_m$ is the optical contrast, and $F(x) = x^{-2}[x^2 - 2x \sin x + 2(1 - \cos x)]$ is the scattering form factor for spherically shaped scatterers derived by Žumer in Ref. [46] using the anomalous diffraction approximation.

From Eq. (10) there is obtained the value of the incidence angle $\theta = \theta_m$ at which the matching condition $m_d(\theta_m) = 1$ is satisfied and a pure PDLC film becomes transparent with $T_{sat}(\theta_m) = 1$. Given the angle θ_m the effective refractive index n_m can now be expressed in terms of the refractive indices n_d^o and n_d^e as follows:

$$n_m^2 = (n_d^o)^2 + \frac{(n_d^o)^2 - (n_d^e)^2}{(n_d^e)^2} \sin^2 \theta_m. \quad (11)$$

Combining the relation (11) with the mixing rule (6) and using Eqs. (2) and (3) gives the equation to be solved for the bipolar order parameter Q_d . This procedure uses the angle θ_m and the volume fractions φ_d and φ_{MNP} as input parameters to estimate the value of Q_d .

The solid line in Fig. 11 shows the theoretical T_s vs θ curve computed for the pure PDLC sample at $\varphi_d = 0.44$, $\varphi_{MNP} = 0.0$, and $\theta_m = 27^\circ$. The above procedure provides an estimate of the bipolar order parameter Q_d at about 0.7. Then the experimental data can be fitted by evaluating the transmittance T_s from Eqs. (7)–(9) and using the radius of the bipolar droplets R_d as a fitting parameter. The value of R_d is found to be about 0.35 μm .

For samples doped with nanoparticles, the treatment, similarly to the case of the pure PDLC film, involves estimating the order parameter Q_d and fitting the experimental data with the radius of the particle aggregates, R_{MNP} , serving as an additional fitting parameter. In Fig. 12 we present the experimental data and theoretical curves for two types of PDLC samples doped with SiO_2 and Sb_2O_5 , respectively.

The estimated value of the order parameter Q_d is about 0.7, which is a typical value for the bipolar orientational structure [38]. For PDLC films in the saturated state, the

estimates of Q_d reported in Refs. [37,38,41] range from 0.6 to 0.86.

The results, shown in Figs. 11 and 12, suggest that doping with nanoparticles does not affect considerably the value of the order parameter Q_d . Therefore, the particles do not disturb the director field inside the bipolar droplets. This counts as corroboration of our conclusion that the particles predominantly form aggregates residing in the polymer matrix. The refractive index of the modified polymer matrix can be estimated from Eqs. (5) and (6). For instance, in the case of a LC-P- Sb_2O_5 composite with $\varphi_p = 35.7$ vol % and $\varphi_{MNP} = 1.3$ vol % (curve 2 in Fig. 12) the refractive index of the pure polymer $n_p = 1.52$ turns out to be increased by 0.01.

IV. CONCLUSIONS

Three-component composites LC-MNP-P form a class of heterogeneous liquid crystal media that show considerable promise for electro-optic applications. The refractive index mismatch between coexisting phases of these composites is shown to be an important factor that affects light scattering and so the electro-optic contrast and its angular dependence. The wide refractive index range of inorganic MNPs allows us to achieve desirable scattering characteristics.

According to the morphology of LC-P systems, two subclasses of LC-MNP-P composites can be selected: (1) a polymer stabilized LC filled with MNPs and (2) a PDLC filled with MNPs. Within the first subclass, the polymer network prevents segregation and reactive fusion which are typical for colloidal MNPs. The electro-optic characteristics of such composites are quite similar to those of LC-aerosil mixtures [11,12]. The off-axis haze of polymer stabilized LC-MNP composites is controllable by the refractive index of the particles. This factor may also have a profound effect on the transmittance in the on state and the isotropic state as well.

The photoinduced phase separation in the LC-MNP-P mixtures with high polymer content ($\varphi_p > 35$ vol %) results in preferential involvement of MNPs in the polymer phase. If the aggregation rate of MNPs is low, the particles do not influence optical uniformity, but modify the refractive index of the polymer. According to both experimental results and theoretical calculations, this modifies the ratio of the refractive indices of LC drops and polymer matrix and, as a result, the scattering characteristics. By this means the electro-optic contrast can be modified and, which is especially important, the off-axis haze of the PDLC can be efficiently suppressed. We believe that the doping of the polymer phase with inorganic MNPs may lead to other improvements of PDLCs, such as enhancement of thermal stability and reduction of LC content in the polymer. Finally, it is demonstrated that MNP doped PDLCs show interesting effects, such as coloring and photochromism. These phenomena attract great attention and open up an interesting field for future studies.

ACKNOWLEDGMENT

These studies were carried out within the framework of the project ‘‘Ordering Regularities and Properties of Nano-Composite Systems’’ of the NASci. of Ukraine.

- [1] *Liquid Crystals: Applications and Uses*, edited by B. Bahadur (World Scientific, Singapore, 1990).
- [2] H. G. Craighead, J. Cheng, and S. Hackwood, *Appl. Phys. Lett.* **40**, 22 (1982).
- [3] F. Aliev, *Access in Nanoporous Materials* (Plenum Press, New York, 1995).
- [4] Paul S. Drzaic, *Liquid Crystal Dispersions*, Series on liquid crystals Vol. 1 (World Scientific, Singapore, 1995).
- [5] D. A. Higgins, *Adv. Mater. (Weinheim, Ger.)* **12**, 251 (2000).
- [6] Y. Fung, D.-K. Yang, S. Ying, L.-C. Chien, S. Zumer, and J. Doane, *Liq. Cryst.* **19**, 797 (1995).
- [7] A. Glushchenko and O. Yaroshchuk, *Mol. Cryst. Liq. Cryst. Sci. Technol., Sect. A* **324**, 45 (1998).
- [8] R. Eidschink and W. Jeu, *Electron. Lett.* **27**, 1195 (1991).
- [9] M. Kreuzer, T. Tschudi, and R. Eidschink, *Mol. Cryst. Liq. Cryst. Sci. Technol., Sect. A* **223**, 219 (1992).
- [10] G. Guba, N. Lopukhov, V. Ogenko, V. Reshetnyak, Yu. Reznikov, and O. Yaroshchuk, *Mol. Cryst. Liq. Cryst. Sci. Technol., Sect. A* **251**, 303 (1994).
- [11] A. Glushchenko, H. Kresse, V. Reshetnyak, Yu. Reznikov, and O. Yaroshchuk, *Liq. Cryst.* **23**, 241 (1997).
- [12] O. Kovalchuk, S. Zakrevska, O. Yaroshchuk, and U. Maschke, *Mol. Cryst. Liq. Cryst. Sci. Technol., Sect. A* **368**, 129 (2001).
- [13] M. Kawasumi, N. Hasegawa, A. Usuki, and A. Okada, *Liq. Cryst.* **21**, 769 (1996).
- [14] A. Yasuda, H. Takanashi, K. Nito, and E. Matsui, *Jpn. J. Appl. Phys., Part 1* **36**, 228 (1997).
- [15] M. Boxtel, R. Janssen, D. Broer, H. Wilderbeek, and C. Bastiaansen, *Adv. Mater. (Weinheim, Ger.)* **12**, 753 (2000).
- [16] M. Boxtel *et al.*, *J. Appl. Phys.* **89**, 838 (2001).
- [17] N. Diorio, M. Fisch, and J. West, *Liq. Cryst.* **29**, 589 (2002).
- [18] Y. Xia, B. Gates, Y. Yin, and Yu Lu, *Adv. Mater. (Weinheim, Ger.)* **12**, 693 (2000).
- [19] L. Dolgov and O. Yaroshchuk, *Colloid Polym. Sci.* **282**(12), 1403 (2004).
- [20] J.-J. Wu and C.-M. Wang, *Phys. Lett. A* **232**, 149 (1997).
- [21] R. Bhargava, S.-Q. Wang, and J. Koenig, *Macromolecules* **32**, 2748 (1999).
- [22] R. Bhargava, S.-Q. Wang, and J. Koenig, *Macromolecules* **32**, 8982 (1999).
- [23] R. Bhargava, S.-Q. Wang, and J. Koenig, *Macromolecules* **32**, 8989 (1999).
- [24] L. Dolgov, O. Yaroshchuk, A. Kovalchuk, and D. S. Wiersma, *Proc. SPIE* **409**, 215 (2004).
- [25] O. Yaroshchuk, L. Dolgov, O. Lavrentovich, and L. Qiu (unpublished).
- [26] L. Dolgov and O. Yaroshchuk, *Mol. Cryst. Liq. Cryst.* **409**, 77 (2004).
- [27] Deeleep K. Rout and Sukhmal C. Jain, *Jpn. J. Appl. Phys., Part 2* **30**, L1412 (1991).
- [28] N. Kambe, S. Kumar, S. Chiruvolu, B. Chaloner-Gill, Y. Blum, D. McQueen, and G. Faris, *MRS Internet J. Nitride Semicond. Res.*, **676**, Y8.22 (2001).
- [29] W. Caseri, *Macromol. Rapid Commun.* **21**, 705 (2000).
- [30] D. Nwabuma, K. J. Kim, Y. Lin, L. C. Chien, and T. Kyu, *Macromolecules* **31**, 6806 (1998).
- [31] V. Sokolov, Yu. Nechepurenko, and G. Branitskiy, *Sov. J. Sci. Appl. Photography* **29**, 59 (1984).
- [32] A. Hagfeldt and M. Graetzel, *Chem. Rev. (Washington, D.C.)* **95**, 49 (1995).
- [33] J.-J. Wu, C.-M. Wang, and S.-H. Chen, *Jpn. J. Appl. Phys., Part 1* **35**, 2681 (1996).
- [34] E. Kaneko, *Liquid Crystal TV Displays: Principles and Applications of Liquid Crystal Displays* (KTK Scientific Publishers, Tokyo, 1987).
- [35] B. G. Wu, J. L. West, and J. W. Doane, *J. Appl. Phys.* **62**, 3925 (1987).
- [36] A. D. Kiselev, O. V. Yaroshchuk, and L. O. Dolgov, *J. Phys.: Condens. Matter* **16**, 7183 (2004).
- [37] F. Basile, F. Bloisi, L. Vicari, and F. Simoni, *Phys. Rev. E* **48**, 432 (1993).
- [38] F. Bloisi, P. Terrecuso, L. Vicari, and F. Simoni, *Mol. Cryst. Liq. Cryst. Sci. Technol., Sect. A* **266**, 229 (1995).
- [39] V. Y. Reshetnyak, T. J. Sluckin, and S. J. Cox, *J. Phys. D* **30**, 3253 (1997).
- [40] S. J. Cox, V. Y. Reshetnyak, and T. J. Sluckin, *J. Phys. D* **31**, 1611 (1998).
- [41] F. Bloisi, C. Ruocchio, P. Terrecuso, and L. Vicari, *Opt. Commun.* **123**, 449 (1996).
- [42] S. J. Cox, V. Y. Reshetnyak, and T. J. Sluckin, *J. Phys. D* **29**, 2459 (1996).
- [43] O. Levy, *Phys. Rev. E* **61**, 5385 (2000).
- [44] P. Sheng, *Introduction to Wave Scattering, Localization and Mesoscopic Phenomena* (Academic, New York, 1995).
- [45] M. C. W. van Rossum and T. M. Nieuwenhuizen, *Rev. Mod. Phys.* **71**, 313 (1999).
- [46] S. Žumer, *Phys. Rev. A* **37**, 4006 (1988).